Aug 11 2021

HLA-E Restricted SARS-CoV-2 Specific T Cells from Convalescent COVID-19 Patients Suppress Virus Replication Despite HLA-Ia Downregulation

Authors: Hong Sun[1,2,3]†, Hongbing Yang[1]†, Simon Brackenridge[1], Xiaodong Zhuang[1], Peter A C Wing[1,2], Max Quastel[1], Lucy Walters[1], Lee Garner[1], Xuan Yao[1,2,4], Suet Ling Felce[1,2], Yanchun Peng[2], Shona Moore[5], Malcolm G. Semple[5,9], Lance C.W. Turtle[5,6], Peter J.M. Openshaw[7], J. Kenneth Baillie[8], Alexander J. Mentzer[9], Paul Klenerman[10], ISARIC-4C Investigators[11], Persephone Borrow[1], Tao Dong[2,4], Jane A McKeating[1,2]*, Geraldine M Gillespie[1]*, Andrew J McMichael[1]*

Affiliations:

1 Nuffield Dept of Clinical Medicine, University of Oxford, NDM Research Building, Old Road Campus, Oxford OX39UT
2 Chinese Academy of Medical Sciences Oxford Institute, NDMRB, Old Road Campus, Oxford OX39UT
3 Key Laboratory of AIDS Immunology, Department of Laboratory Medicine, First Affiliated Hospital of China Medical University, Shenyang, China
4 MRC Human Immunology Unit, MRC Weatherall Institute of Molecular Medicine, Oxford University
5 Health Protection Research Unit in Emerging and Zoonotic Infections, Institute of Infection, Veterinary and Ecological Sciences, University of Liverpool
6 Tropical & Infectious Disease Unit, Liverpool University Hospitals NHS Foundation Trust (member of Liverpool Health Partners)
7 National Heart and Lung Institute, Imperial College London, London
8 Roslin Institute, University of Edinburgh, Edinburgh,
9 Wellcome Centre for Human Genetics, University of Oxford, Old Road Campus, Oxford OX3 7BN
10 Peter Medawar Building for Pathogen Research and Translational Gastroenterology Unit, University of Oxford
11 International Severe Acute Respiratory Infection Consortium- Coronavirus Clinical Characterisation Consortium. https://isaric4c.net/about/authors/

*Corresponding authors:
Email: Andrew J McMichael, andrew.mcmichael@ndm.ox.ac.uk; Geraldine M Gillespie, geraldine.gillespie@ndm.ox.ac.uk; Jane A McKeating, jane.mckeating@ndm.ox.ac.uk

† These authors contributed equally

Abstract: Pathogen specific CD8 T cell responses restricted by the non-polymorphic non-classical MHC class Ib molecule HLA-E are rare in human infections. Epitope peptides have to compete for binding to HLA-E with the natural ligand, a signal peptide derived from classical class I HLA molecules that interacts with the NKG2/CD94 receptors to regulate natural killer (NK) cell functions. Here we describe five epitope peptides from severe acute respiratory syndrome coronavirus 2 (SARS-CoV-2) that elicited HLA-E restricted CD8 T cell responses in COVID-19 convalescent patients. These T cell responses were present in the blood at levels similar to those reported for classical HLA-Ia-restricted anti-SARS-CoV-2 CD8 T cells. Peptide specific CD8 T cell clones, which expressed diverse T cell receptors, suppressed SARS-CoV-2 replication in Calu3 human lung epithelial cells. SARS-CoV-2 infection markedly downregulated classical HLA class I expression in Calu3 cells whereas HLA-E expression was enhanced, enabling T cell recognition. Thus HLA-E restricted T cells could have an advantage over classical T cells in controlling early SARS-CoV-2 infection.

One Sentence Summary:

SARS-CoV-2 restricted HLA-E restricted CD8 T cells, that are able to suppress virus replication in vitro despite classical HLA Class I down-regulation, are present in COVID-19 convalescent patients.

Main Text:

INTRODUCTION

Unlike the genetically polymorphic classical HLA A,B and C molecules, just two major HLA-E allomorphs dominate at the population level, differing in a single amino acid at position 107 outside the peptide binding groove (*1*). HLA-E is expressed on the surface of most cells at 1-5% of the level of the classical HLA A and B molecules but is also present intracellularly (*2-4*). There is some variation in different tissues, with higher levels on cells of lymphoid, renal and lung tissues (https://www.proteinatlas.org/ENSG00000204592-HLA-E/tissue). The primary role of HLA-E is to present a well conserved nonamer peptide, typically VMAPRTLVL (VL9), derived from the signal sequence of classical major histocompatibility complex class-Ia (MHC-Ia) molecules, to the natural killer cell receptors CD94-NKG2A and CD94-NKG2C (*5*). The former binds with higher affinity and delivers a dominant inhibitory signal to natural killer (NK) cells and to a subset of CD8+ T cells, regulating their activity. Conservation of the signal peptide sequence and of the structure of the MHC-E peptide binding groove between mammalian species imply a common evolutionary origin for this important immune function. The signal peptide normally dominates the HLA-E bound peptidome, in contrast to the diverse peptide repertoire bound to the polymorphic classical HLA class Ia molecules (*6*).

MHC-E can also present pathogen derived peptides and altered self peptides to CD8+ T cells, like classical MHC- Ia molecules (*7-10*). However, nearly all reported antigenic peptide epitopes bind HLA-E with markedly lower affinity than the VL9 signal peptide (*11, 12*) and consequently are likely to be out-competed by VL9 for binding to HLA-E in the endoplasmic reticulum (ER). It is not surprising therefore that relatively few HLA-E restricted T cell responses have been described. However, if generation of, or access to, the VL9 signal peptide

is impaired or bypassed, other peptides can gain access to HLA-E and stimulate CD8+ T cell responses. Strong MHC-E restricted T cell responses have been reported in a few specific settings. One example is in rhesus monkeys following vaccination with Simian Immunodeficiency Virus (SIV) immunogens vectored by a particular strain of rhesus monkey cytomegalovirus (RhCMV68-1) (*7*). This CMV vector has gene deletions (*13*) that alter virus tropism, while retaining genes that interfere with key elements of the classical antigen processing pathway that delivers the host cell's VL9 signal peptide to MHC-E. Instead, a viral-derived VL9 peptide binds to MHC-E in the ER enabling the complex to traffic to the cell surface, where MHC-E is subsequently internalised and most likely gains access to other peptides within endosomes (*14*). These infected cells then prime CD8+ T cells (*13, 14*) that are uniquely able to quench a challenge infection with SIV (*7, 14*). A second example is in human mycobacterial infections where antigen processing and HLA-E peptide binding occur in the phagolysosomes of infected macrophages rather than in the ER (*15*). Most adult humans have readily detectable HLA-E restricted mycobacteria specific T cells in their blood (*9*).

In this study we assessed whether HLA-E restricted T cells could contribute to the complex immune responses to SARS-CoV-2. We found that there were readily detectable, previously unrecognized, CD8+ T cell responses to viral peptides presented by HLA-E in convalescent patients. Furthermore, these T cells were able to suppress virus replication in an experimentally infected human lung epithelial cell line. In addition, we found that SARS-CoV-2 down-regulated surface expression of classical HLA class Ia molecule while transiently enhancing expression of HLA-E.

RESULTS

Identification of SARS-CoV-2-derived HLA-E binding peptides

Twenty-nine nonamer SARS-CoV-2 peptides (Table S1) derived from all open reading frames annotated in the reference genome (NC_045512.2) that were predicted to bind HLA-E by NetMHC4.0 (*16*) or by an in-house binding data informed algorithm (*11*) (Table S1) were selected for evaluation. Peptides P001–P010 represent the top HLA-E binders predicted by NetMHC4.0 (*16*). Peptides P011–P029 were selected from 216 predicted peptides that possessed the HLA-E peptide binding motif previously reported (*12*). This requires hydrophobic primary anchor residues at position 2 [M, I, L, V, A, F or Q] and position 9 [L, F, I, V or M], plus the presence of a proline between positions 3 and 7 of the peptide. All peptides were tested for binding to HLA-E by a UV peptide-exchange enzyme-linked immunosorbent assay (ELISA) (*11*) and single chain peptide-β2m-HLA-E trimer (SCT) cell surface expression (*7*). Peptide binding data generated by these two independent assays showed good agreement (Fig. 1A) for peptides with the strongest binding signals – which included four predicted by NetMHC4.0 and two from our modified algorithm (*11, 12*).

HLA-E-peptide complexes were stabilised by keeping a molar excess of peptide in the protein buffer. The five highest binding SARS CoV-2 peptides were further validated by differential scanning fluorimetry (DSF) to assess the thermal stability of HLA-E bound to these peptides (*12*). These data indicated that peptide 001, VMPLSAPTL, bound to HLA-E almost as well as VL9, so that stable conventional refolded tetramers could be made, whereas the other peptides bound in the range where they required stabilization by maintenance in a molar excess of peptide. This was achieved by using the method of UV exchange method to introduce individual peptides into HLA-E initially refolded with an UV sensitive version of the VL9

peptide, and then maintaining these samples in molar excess peptide following tetramerization and throughout storage (*11, 17*). In this way we were able to generate five stable HLA-E-peptide tetramers that bound T cell receptors with sufficient avidity to enable detection by flow cytometry(*12*).

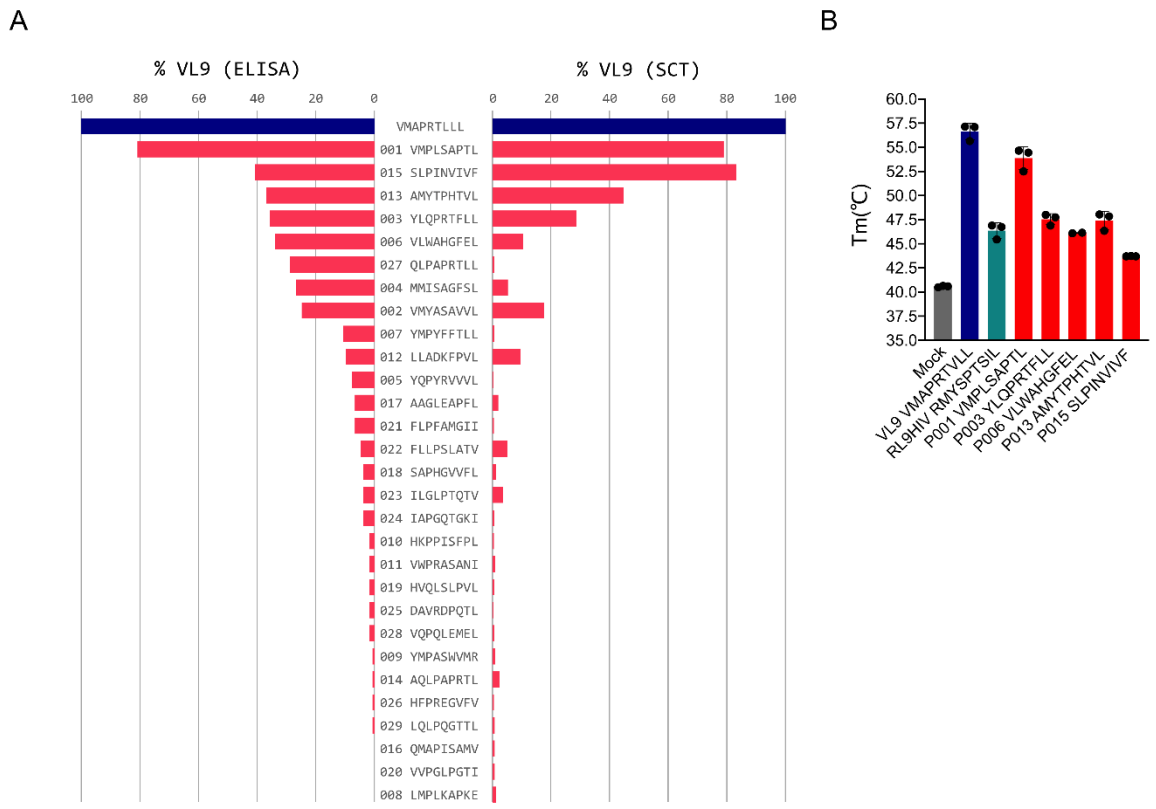

Fig. 1 Identification of HLA-E binding peptides using multiple strategies

(**A**) NetMHC and in-house algorithm predicted SARS-CoV-2 derived-peptides were screened using both a UV peptide-exchange HLA-E binding ELISA assay and a single-chain trimer (SCT) HLA-E cell-surface expression assay. For ELISA assay-derived binding data, the percentage of absorbance signals for individual peptides were normalized to the VL9 positive control signals (%VL9) to rank HLA-E binding strength. For the SCT assay, the mean intensity for each tested peptide was normalized to that of the VL9 (%VL9) control. Tested peptide, red; VL9, positive control, dark blue. For ELISA-based screens, three independent peptide exchange reactions were performed per individual peptide (n=3), with 2 technical replicas per peptide tested in ELISA screens. The SCT assay was performed in triplicate. (**B**), The thermal melt temperatures (Tm) of peptide-free HLA-E-β2m complexes pulsed with 100M excess of the top 5 ELISA-ranked SARS-CoV-2 peptide binders were determined by differential scanning fluorimetry (DSF). The positive control VL9 peptide and the previously reported HLA-E binding peptide, RL9HIV, were included for reference. SARS-CoV-2 peptide HLA-E, red; HIV Gag RL9, green; VL9, blue; mock, grey.

HLA-E restricted SARS-CoV-2-specific CD8+ T cells in convalescent COVID-19 patients

We employed five HLA-E SARS-CoV-2 peptide tetramers (P001, P003, P006, P013 and P015) to investigate whether SARS-CoV-2 specific CD8 cells could be detected in convalescent COVID-19 patients. Tetramer positive cells were gated on live CD3+CD4-CD8+ singlets which were $CD56^-$ and $CD94^-$ to exclude NKG2/CD94 receptor expressing cells (Fig. S1A). We further excluded NKG2 receptor binding by making NKG2A and NKG2C tetramers and showing that they failed to bind to SARS-CoV-2 peptide SCTs expressed on transfected 293T cells, in contrast to the VL9 SCT control (Fig. S1B).

Peripheral blood mononuclear cells (PBMCs) from 9 healthy donors collected in 2019 prior to the Covid-19 pandemic were stained with these HLA-E tetramers to establish the level of background staining from naïve donors. The mean + 2 standard deviations (SD) gave a threshold for positive staining of >0.09% of CD8+ T cells (Fig. 2A).

In an initial study, we stained PBMCs from 5 COVID-19 convalescent patients, 3 sampled after mild infection (presenting to hospital early in the pandemic but never requiring oxygen) and 2 after recovering from severe disease, requiring supplemental oxygen but not assisted ventilation, enrolled at the John Radcliffe Hospital in Oxford (Table S2). HLA-A2 negative patients were selected to avoid HLA-A2-mediated presentation of the peptide epitopes because HLA-E and HLA-A2 share an overlapping peptide binding motif (*18*). SARS-CoV-2-specific CD8+ T cells for 3 different peptides (P001, P006 and P015) were identified, with differences observed between patients in terms of the magnitudes (0.1-0.6% of CD8+ T cells) and breadth of responses (Fig. 2B).

The finding that HLA-E restricted CD8 responses were detectable at levels comparable to those of conventional HLA Ia-restricted T cells in PBMC of convalescent patients (*19-24*) led us to study a larger group of 22 convalescent patients, recruited in Liverpool on the ISARIC4C

clinical characterisation protocol (CCP01118-02366 in Table S1). These patients were stratified into those recovering from mild (n=8) or more severe disease (n=14), where the latter group experienced intensive treatment unit (ITU) admission and/or required oxygen before disease resolution. Patients from both cohorts did not differ in age or time post symptom onset when considering severity categories (Fig. S2). HLA-E tetramer positive CD8+ T cells were detected in PBMCs from 18 patients, with a mean frequency of 0.22% CD8+ T cells (IQR, 0.10%-0.39%). These frequencies are comparable to those of classical HLA Class Ia restricted SARS-CoV-2 specific T cells reported previously (*19, 20, 22-25*). We noted that the frequencies of tetramer positive CD8+ T cells were significantly lower in patients who recovered from mild infections, 0.11% (IQR, 0.00%-0.23%), compared with severe convalescent patients, 0.30% (IQR, 0.12%-0.52%) (p= 0.03, Mann Whitney U test, Fig. 2C). In addition, the number of tetramers that gave detectable staining of CD8+ T cells was greater in the severe disease group. Peptide P001 staining, which was detected in 14 patients, was the most common epitope recognised, but the frequency of P001-tetramer binding cells by itself did not accurately reflect the total response (Fig. 2C). These findings suggest that higher levels of virus exposure in severe patients (*26, 27*) elicited HLA-E restricted T cell responses that were of higher magnitude and broader, at least in those that recovered from their infection, than those in patients with mild disease.

In order to explore the antiviral functions of HLA-E restricted SARS-CoV-2 specific T cells, we generated SARS-CoV-2 specific HLA-E restricted CD8+ T cell clones. CD8 positive PBMCs from two convalescent patients, Pt1016 (mild disease) and Pt1504 (severe disease), were stained with a mixture of three HLA-E tetramers (peptides P001, P006 and P015). Tetramer positive CD8+ T cells were sorted and seeded at <0.4 cells per well in microtiter trays and cultured with irradiated allogeneic feeder cells, phytohaemagglutinin (PHA) and

interleukin-2 (IL-2). 87 clones proliferated and HLA-E tetramer staining revealed 9 positive clones from Pt1016 and 4 positive clones from Pt1504 (Fig. 2D). When co-stained with single peptide HLA-E tetramers labelled with different fluorophores, each clone demonstrated single peptide specificity (Fig. 2E, 2F). 8 of 13 clones were specific for peptide P015, whereas 3 clones were peptide P001 specific and 2 clones were specific for peptide P006 (Fig. 2F). This finding ruled out non-specific binding to HLA-E through their TCRs or other receptors.

The T cell receptors (TCRs) of the clones were sequenced using the SMART (Switching Mechanism at 5'end of RNA Template) (*28*) and 5'RACE (5'Rapid Amplification of cDNA Ends) techniques (*29*). Each expressed a single TCR β chain, while 3 out of 13 clones expressed two alpha chains (Table 1). The TCRs were diverse, but two of three P001 specific T cell clones used TRAV21 and 3 out of 8 P015 specific clones utilized TRBJ2-1.

The frequency of tetramer positive cells within the 13 clones ranged from 0.7%-43% of CD8+T cells (Fig. 2D, Table S3). Those with <5% staining were considered to be equivocally SARS-CoV-2 specific; although they were clonal populations they may have had other primary specificities with weak additional cross reactivity with peptide-HLA-E complexes. Those with higher binding were likely have high peptide-HLA-E specificity. Incomplete tetramer staining has been previously reported for HLA-E-restricted HIV-1 specific CD8+ T cell clones (*30*) and also for T cells detected with MHC Class Ia-peptide tetramers (*31, 32*). Stable binding by tetramers depends on the avidity conferred by two or more of the HLA-E-peptide complexes within the tetramer binding to TCRs on T cells. If overall TCR density is low, T cells at the lower end of the Gaussian distribution would bind only one of the four HLA-E-peptide components of the tetramer, so that binding would be dependent on affinity, which is low for TCRs (*33-35*). T cells with higher TCR density could bind two or more peptide-HLA

complexes within the tetramer, gaining avidity; for antibodies this can increase binding >100-fold (*36*). When the wash step after initial tetramer binding(*37*), before addition of anti-CD8 antibodies, was eliminated higher levels of staining were observed (Fig. S1C, D).

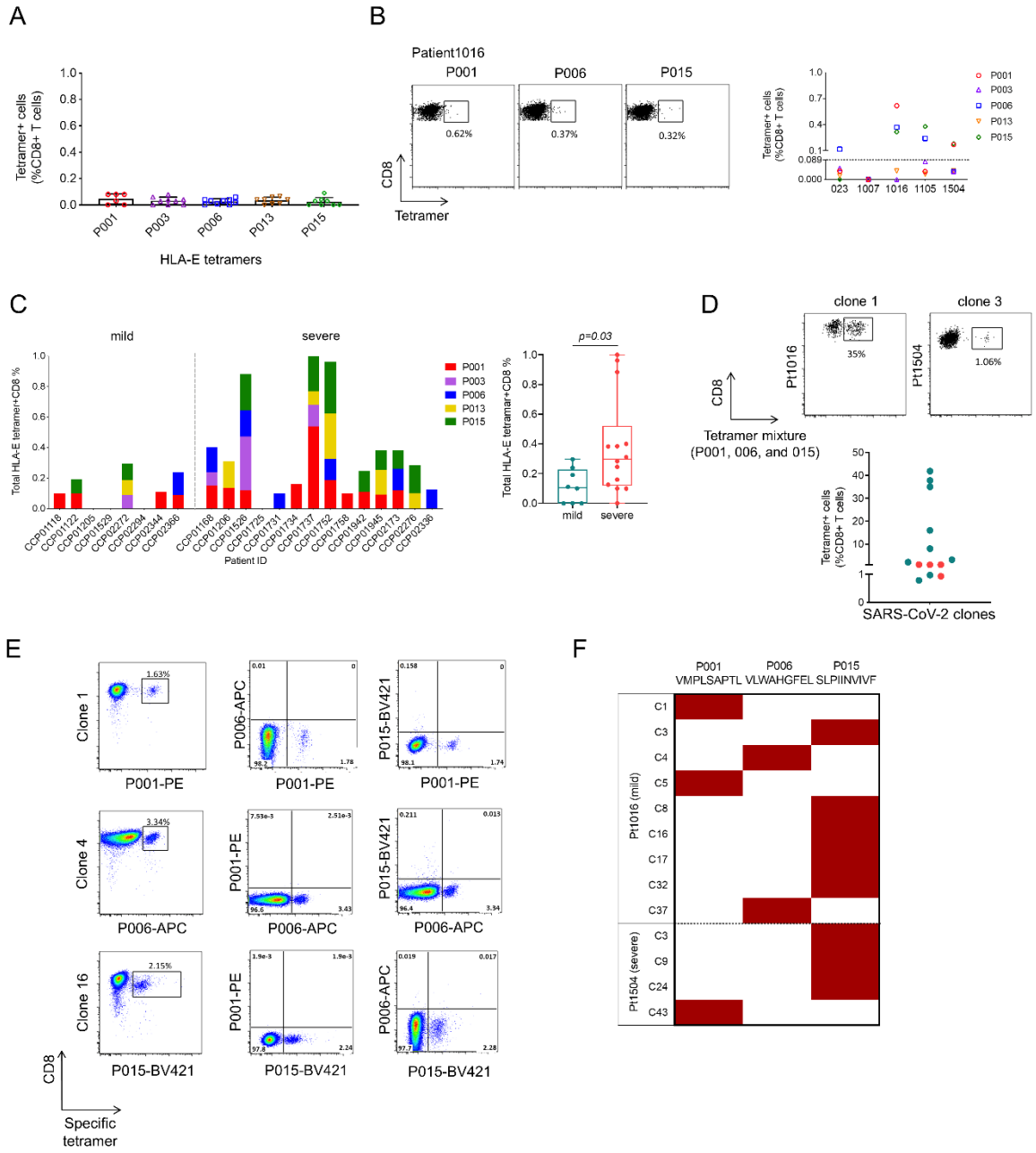

Fig. 2 HLA-E restricted SARS-CoV-2-specific CD8+ T cells in convalescent COVID-19 patients

(A) The frequencies of CD8 tetramer+ cells from healthy donors (n=9) collected prior to the COVID-19 pandemic are plotted against different HLA-E-SARS-CoV-2 tetramers (x-axis). Threshold of positive tetramer staining was calculated as values falling above the mean+2 standard deviations (SD). **(B)** *Ex vivo* tetramer staining was performed initially on PBMCs from convalescent patients from the John Radcliffe Hospital in Oxford (n=5). Representative FACs plots (Pt1016) indicate tetramer^{+}CD8^{+}T cells following the gating described in **Fig. S1A**. The frequencies CD8 tetramer^{+} cells from convalescent patients (n=5) are summarized, with the % frequencies obtained with the 5 different HLA-E tetramers denoted using distinct symbols. The dotted line indicates the cut-

off threshold for tetramer positivity. **(C)** Tetramer^{+}CD8^{+} T cell responses for the top 5 ELISA-ranked HLA-E binding peptide was evaluated in the ISARIC convalescent cohort (n=22). Summed tetramer^{+}CD8^{+}T cell frequencies are plotted against patient identifiers (left) and disease severity (right). Severe, red dots; mild, green dots. Significance was calculated using Mann-Whitney test. **(D)** Representative flow graphs depicting the tetramer staining of SARS-CoV-2 specific CD8 clones. The frequencies of all 13 clones are displayed. Pt1016 clones, green dots; pt1504 clones, red dots. **(E)** Representative FACS plots demonstrating the tetramer-specificity of individual SARS-CoV-2 CD8 clones evaluated using tetramers tagged with different fluorochromes (P001/PE, P006/APC and P015/BV421) is shown. **(F)** A heatmap summarizing the peptide specificity of each CD8 clone is presented, where each row denotes separate CD8 clones, and each column represents individual HLA-E SARS-CoV-2 peptides (P001, P006 and P015).

Functions of HLA-E restricted SARS-CoV-2-specific CD8+ T cells

The functions of the 13 SARS-CoV-2 specific CD8 clones were assessed by measuring expression of cytokines (IFN-γ, TNF-α, MIP1β; IL-4, IL-13), cytolytic proteins (CD107a/b, Granzyme a/b), activation molecules (CD137) and inhibitory molecules (CTLA-4) following peptide stimulation. The antigen presenting cells comprised peptide pulsed HLA-E-transduced K562 cells, an erythroleukemia cell line that lacks endogenous HLA class I (*18*). We observed peptide specific cytolytic degranulation and activation, as defined by CD107a/b and CD137 expression respectively, for most CD8 clones (Fig. 3A). We also evaluated maximal functionality following PMA/Ionomycin stimulation. The clones from Pt1504, the severe disease donor, produced significantly less IFN-γ, higher IL-13 and expressed elevated CTLA-4 relative to those from Pt1016 (Fig. 3B). Future studies with a larger patient cohort will determine whether such differences associate with disease severity.

We then asked whether the T cell clones recognise SARS-CoV-2 infected cells. A viral suppression assay (VSA) was designed using the respiratory epithelial Calu-3 cell line that has been widely used to study SARS-CoV-2 infection (*38, 39*). T cell clones were co-cultured with SARS-CoV-2 (Victoria 01/20 strain) infected Calu-3 cells at an effector: target (E:T) ratios of 1:1 and 4:1 for 15 hours to ensure robust virus replication (Fig. 3C). Two CD8+ T cell clones that were completely negative for tetramer staining, although isolated from a SARS-CoV-2 convalescent patient, were used as controls alongside HLA-E-restricted HIV-1 specific CD8+ T cell clones (*30*). We assessed antiviral activity by measuring SARS-CoV-2 replication by RT-qPCR evaluation of viral RNA (*40*).

We confirmed that uninfected Calu-3 cells expressed HLA-E at a comparable level to PBMCs (Fig. S3), making it possible for these cells to present SARS-CoV-2 epitopes to CD8+ T cells.

When HLA-E-restricted SARS-CoV-2 specific clones were cultured with the infected Calu-3 cells, we found significantly reduced levels of viral RNA compared to control clones (Fig. 3C-F). T cell clones from the two convalescent patients Pt1016 and Pt1504 inhibited viral RNA transcription at an E:T ratio of 1:1, when compared to control clones (Fig. 3D) and this antiviral effect was enhanced at an E:T ratio of 4:1, when clones from Pt1016 mediated 94% mean inhibition of viral replication (Fig. 3E-F). Thus HLA-E restricted SARS-CoV-2 specific T cells were capable of recognizing infected cells and suppressing virus replication.

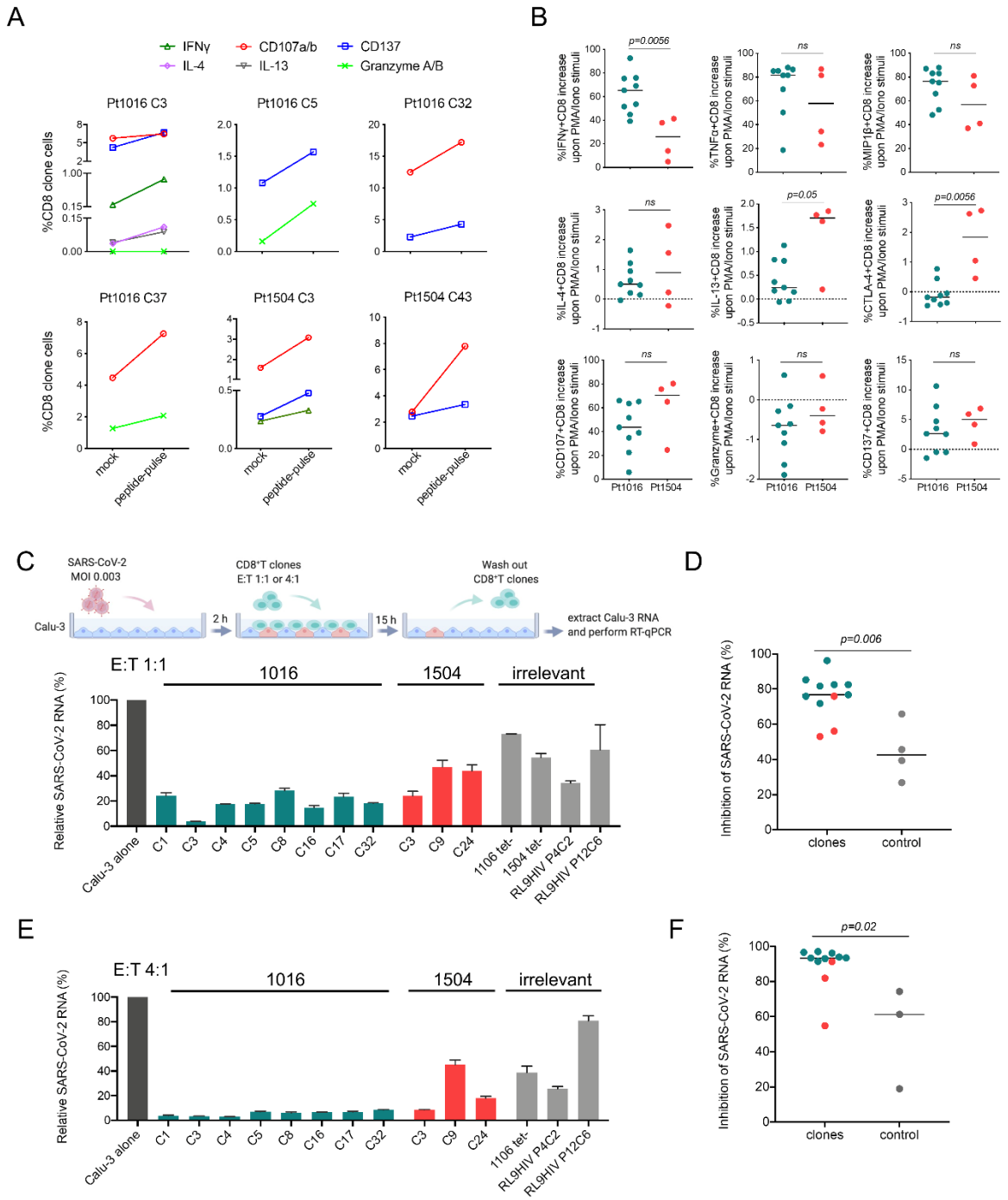

Fig. 3 Characterization of the functionalities of HLA-E restricted SARS-CoV-2 specific CD8 clones

(A) The upregulation of functional molecules including IFNγ, TNFα, MIP-1β, IL-4, IL-13, CTLA-4, CD107a/b, Granzyme a/b and CD137 on T cell clones following incubation with mock (no peptide) and peptide pulsed HLA-E transduced K562 cells was assessed. (IFNγ, green triangle; CD107a/b, red circle; CD137, blue square; IL-4, purple diamond; IL-13, inverted triangle; Granzyme a/b, light green cross) **(B)** The up-regulation of functional molecules expressed by T cell clones following PMA/Ionomycin. Patient ID is indicated on the X-axis and

functional readout on the y-axis. Statistical significance was calculated using Mann Whitney test. **C-F,** The antiviral capacity of SARS-CoV-2 specific T cell clones was assessed in a viral suppression assay (VSA): intra-cellular viral transcription in Calu-3 infected cells was analyzed using RT-qPCR after co-culture with CD8+ T cell clones. Relative expression of viral transcription normalized to SARS-CoV-2 infected Calu-3 cells is depicted on y-axis. The degree of inhibition, reported as % relative SARS-CoV2 RNA, was compared between clones from patients Pt1016 and Pt1504, patient-derived control T cell clones that did not stain with HLA-E-SARS-CoV-2 tetramers and two HLA-E-restricted clone specific for the HIV-1 Gag RL9 peptide (RL9HIV). The workflow of the VSA is depicted above **(C)** (created in BioRender.com). Viral suppression at E:T 1:1 (**C-D**) and E:T 4:1 (**E-F)** are presented. Pt1016, green bars/dots; Pt1504, red bars/dots; irrelevant: shade bars/dots. Data shown are representative of three independent experiments. Significance was calculated using Mann Whitney test.

SARS-CoV-2 infection perturbs HLA-E and HLA-I expression

Finally, we investigated whether HLA-E restricted T cell responses were influenced by SARS-CoV-2 induced downregulation of HLA-I expression (*41*). We monitored infection by quantifying expression of the viral encoded Spike glycoprotein and observed an increasing frequency of Spike positive cells over time consistent with a spreading infection (Fig. 4A-B). We confirmed that Spike expression was dependent on virus replication, as treating cells with Remdesivir (RDV), a ribonucleotide inhibitor of RNA-dependent RNA polymerase, ablated Spike expression (Fig. 4A-B). SARS-CoV-2 infected Spike positive cells showed an increase in cell surface HLA-E expression and reduced levels of HLA-I compared to uninfected cells and this phenotype was eliminated by RDV treatment (Fig. 4C, Fig. S4). Infecting the cells with differing amounts of virus (MOI of 0.1 and 1) showed a dose-dependent virus modulation of both surface and total HLA-E and HLA-I expression (Fig. 4D-F). At 48 hours post-infection (hpi), when cells infected at MOIs of 0.01 were evaluated, as cell cultures infected at higher MOI exhibited substantial cytopathic effects at this time point, HLA-I expression was dramatically reduced in spike positive compared to negative cells. In contrast, HLA-E expression was only marginally reduced at this time (Fig. 4G, H). Furthermore, we noted a time-dependency in virus perturbation of HLA expression (Fig. 4F). We obtained similar results using an independent lung epithelial A549 cell line engineered to express ACE2 (A549-ACE2) (*42*). We noted similar infection rates with comparable Spike expression over time with similar perturbations in HLA-I and HLA-E expression (Fig. S5).

Two recent studies provide a potential explanation for the downregulation of class I HLA in SARS CoV-2 infected cells. Zhang et al (*41*) show that the virus ORF8 gene product targets HLA-class I molecules for autophagy and degradation, thereby reducing total HLA-I expression; here we showed that HLA-E escapes this downregulation. Hsu et al et al (*43*)

showed that SARS CoV-2 infection rapidly shuts down host protein translation, a process dependent on NSP14. This mechanism is likely to impact on classical antigen processing where peptides transported by the transporter associated with antigen processing (TAP) from the cytosol to the peptide loading complex in the ER, bind to newly synthesised HLA class I molecules, which then traffic to the cell surface. If this translational block is rapid and followed by degradation of any escaping intracellular MHC class I molecules by ORF8, only HLA class I proteins generated before infection would remain on the cell surface until they decay, with a half-life of approximately 3 hours (*44*). Classical HLA class I molecules are unstable in the absence of peptide and degradation is accelerated by acidification, which releases peptide, in endosomes after internalization. In contrast, HLA-E-β2m dimers are relatively stable in the absence of peptide and can exist in intermediate folded forms that are receptive to peptide binding (*11, 12, 45*). MHC-E is also relatively abundant intracellularly (*4*) (confirmed in Fig. 4D) suggesting an intracellular store that traffics to the cell surface more slowly. In addition, MHC-E can acquire epitope peptides in endosomes after internalization of MHC-E carrying the signal VL9 peptide, before recycling to the cell surface (*14*). Similarly, Grotzke et al (*15*) showed that mycobacterial peptides bind HLA-E in the phagolysosome and recycle to the cell surface of macrophages, a process that continues when host cell protein synthesis is blocked. In contrast, classical HLA-I antigen processing was abrogated by shutting down host protein synthesis. Thus, in these diverse infections, SARS-CoV-2, RhCMV68-1 and Mycobacterium tuberculosis, disturbance of classical antigen processing can favor MHC-E peptide binding and emergence of MHC-E restricted T cell responses. The relatively high levels of HLA-E in the lower respiratory tract (https://www.proteinatlas.org/ENSG00000204592-HLA-E/tissue), could also contribute to the unusually high frequency of HLA-E restricted T cell responses in SARS Co-V-2 infection.

HLA A, B and C restricted CD8+ T cells should still be primed by cross presentation of non-infectious viral products taken up by dendritic cells (*46*). This could explain why the classical T cell responses are present at very similar levels to the HLA-E restricted T cell frequencies seen here, after SARS CoV-2 infection (*19-24*). The former could retain some activity on recently infected cells, especially if the translational and post translational blocks are incomplete, whereas the latter could be effective for longer. The relative protective activities of HLA-E restricted compared to HLA-Ia restricted T cells remain to be determined, but it is likely that the normal balance, which is strongly in favour of classically restricted T cells, is disturbed in SARS-CoV-2 infection and that HLA-E-restriction could be equally important in this specific setting. Future studies will address this question in detail.

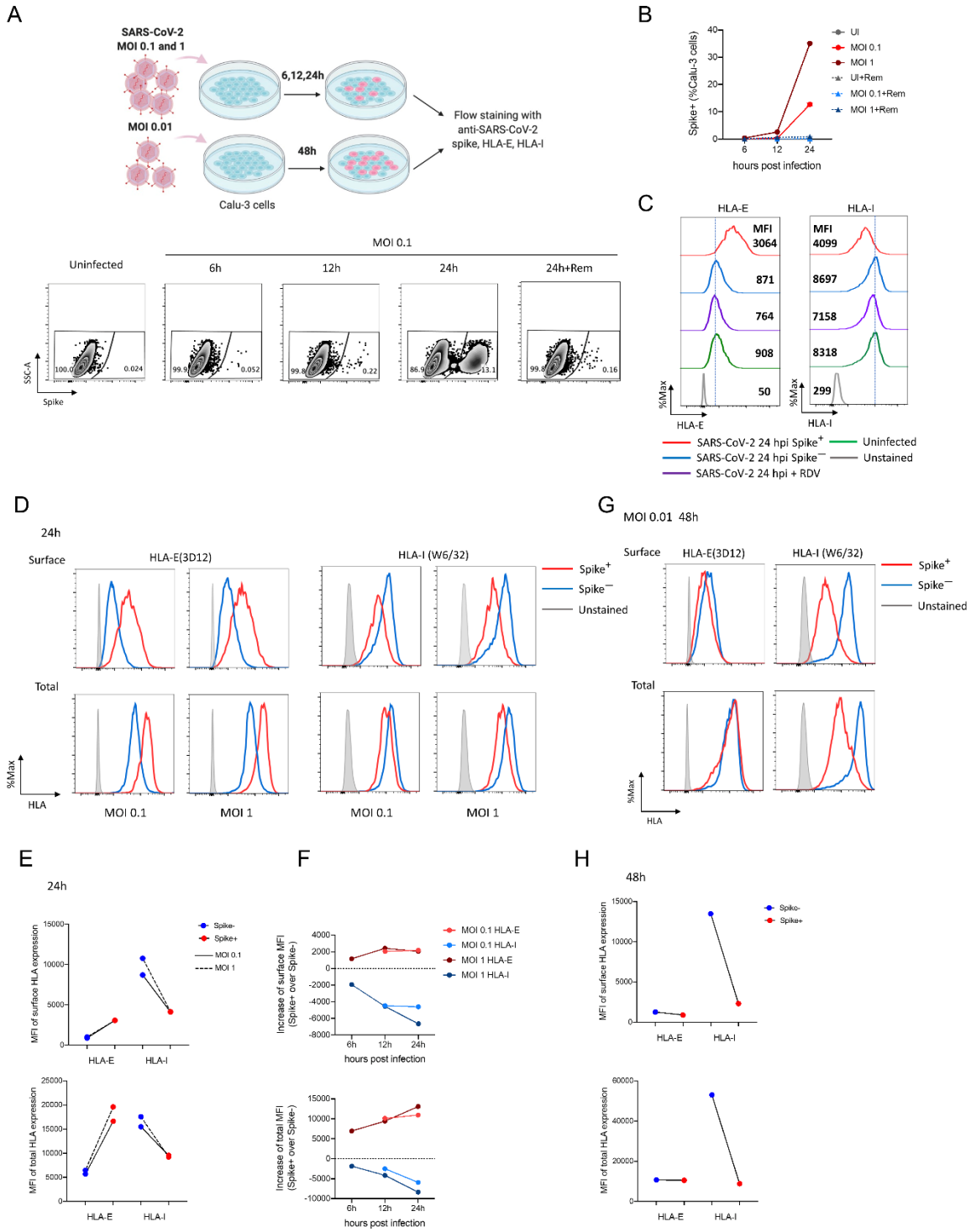

Fig. 4 HLA-E and HLA-I dysregulation in Calu-3 cells upon SARS-CoV-2 infection

(A-B) Replication dynamics of SARS-CoV-2 in Calu-3 cells was assessed using an anti-SARS-CoV-2 spike antibody following infection of WT SARS-CoV-2 virus at different MOIs and timepoints following infection: MOI 1 and 0.1 at 6, 12, 24 hpi, or MOI 0.01 at 48hpi. **(A)** The infection and evaluation workflow is depicted

(upper diagram, created in BioRender.com). Representative graphs depict spike^{+} cells, assessed by intracellular (ICS) staining at a MOI 0.1 (represented as SSC versus spike). 2 hours after viral infection, Remdesivir (Rem) was added. **(B)** SARS-CoV-2 infection kinetics for Calu-3 cells at the indicated timepoints is depicted. MOI 1, cayenne; MOI 0.1, red; MOI 1 with Remdesivir treatment, ocean; MOI 0.1 with Remdesivir treatment, blue; uninfected (UI), grey. Remdesivir addition, triangle. **(C)** HLA-E and HLA-I surface expression, assessed by anti-3D12 and anti-W6/32 staining respectively, for each condition at 24hpi and MOI 0.1 is shown. Spike+, red; Spike-, blue; Remdesivir, purple; Uninfected control, green; Unstained, grey. The Median Fluorescent Intensity (MFI) is indicated. **(D)** Representative histograms (MOI 0.1 and 1) denote HLA expression (MFI) of spike+ and spike- cells on the surface (above) and in total (below) at 24hpi. Spike+, red; spike-, blue; unstained control, grey. **(E)** MFI of HLA expression between spike+ and spike- cells are compared. MOI 0.1, solid line; MOI 1, dash line; spike+, red; spike-, blue. **(F)** HLA-E and HLA-I expression in spike+ versus spike- cells change dynamically along with time. MOI 0.1, red (HLA-E) and blue (HLA-I); MOI 1, cayenne (HLA-E) and ocean (HLA-I). **(G)** Representative histograms (MOI 0.01) denote HLA expression of spike+ and spike- cells on the surface (above) and in total (below) at 48hpi. **(H)** MFI of HLA expression between spike+ and spike- cells are compared. Spike+, red; spike-, blue. Data shown are representative of two independent experiments.

Materials and Methods:

Study Design

The project aimed to elucidate the presence of HLA-E restricted CD8 response in convalescent COVID-19 patients using HLA-E tetramers in complex with 5 SARS-CoV-2 derived peptides. HLA-E restricted CD8+ T cell clones generated from the patients in response to these peptides demonstrated antiviral activity against SARS-CoV-2 infected Calu-3 cells. SARS-CoV-2 infection downregulated classical HLA-I expression *in vitro* while HLA-E expression remained unaltered, thereby potentially explaining why increased frequencies of HLA-E restricted T cells against SARS-Co2-derived epitopes exist *in vivo*.

Study participants and ethical approvals

Five convalescent COVID-19 patients in the pilot study were enrolled in the John Radcliffe Hospital in Oxford described previously (*22*) while 22 convalescent COVID-19 patients were recruited from University of Liverpool from the International Severe Acute Respiratory and Emerging Infections Consortium (ISARIC)/World Health Organization (WHO) Clinical Characterisation Protocol for severe emerging infection UK (CCP-UK) cohort study (Study registration ISRCTN66726260 https://doi.org/10.1186/ISRCTN66726260).

For clinical stratification of these patients, mild disease is defined as no oxygen requirement and no admission onto the intensive treatment unit (ITU) survived to discharge and. Severe disease is defined as any requirement for oxygen, or receipt of Continuous Positive Airway Pressure (CPAP) or high flow oxygen, admission onto the ITU or death.

The study was approved by South Central–Oxford C Research Ethics Committee in England (reference: 13/SC/0149) and Scotland A Research Ethics Committee (reference: 20/SS/0028) and World Health Organization Ethics Review Committee (RPC571 and RPC572l; 25 April 2013). All participants have signed the informed consent.

Peptides

Synthetic 9 amino acid SARS-CoV-2 derived peptides and HLA-B leader sequence peptide VMAPRTVLL (VL9), were synthesized by Genscript (>85% purity). A UV-labile HLA-B leader-based peptide (VMAPRTLVL) incorporating a 3-amino-3-(2-nitrophenyl)-propionic acid residue substitution at position 5 (J residue) was synthesised by Dris Elatmioui at Leiden University Medical Centre, The Netherlands. Lyophilized peptides were initially reconstituted to 200mM or 100mM in DMSO and aliquoted for cryopreservation at -80C° until further use.

Protein expression, purification and refolding

The details of HLA-E heavy chain expression, inclusion body preparation-solubilisation, refolding and final purification were performed according to protocols have been previously described (*5, 7, 11, 12, 30*).

Differential scanning fluorimetry

The thermal stability of no-peptide and peptide-loaded HLA-E was determined by differential scanning fluorimetry (DSF) using Prometheus NT.48 Series instrumentation (Nanotemper). Assay design was based on a previously published method (*47*). In brief, 0.45 μg/μL of HLA-E was incubated with 100M excess peptide in a 20μL final volume of 50mM Tris pH 7, 150mM NaCl buffer for 30 minutes. Following incubation, approximately 20μL of individual samples were split between two Prometheus NT.48 Series nanoDSF Grade Standard Capillaries (Nanotemper, Munich, Germany) and transferred into a capillary sample holder. Excitation power was pre-adjusted to obtain a range between 8000 and 15,000 Raw Fluorescence Units for fluorescence emission detection at 330 nm and 350 nm. A thermal ramp

of 1 °C/min from 20 °C to 95 °C was applied. Thermal melt data calling was automatically generated using the analysis software within PR.ThermControl software version 2.1.5.

Cell lines and primary cells

The MHC-I null cell line K562 transfected with HLA-E*01:03 (K562-E line) was kindly provided by Thorbald van Hall (LUMC) (*18*) . Calu-3 were provided from Anderson Ryan (Oncology Department, University of Oxford) and A549-ACE2 cells were provided by Alfredo Castello (CVR, University of Glasgow) (*40*). PBMCs were isolated from healthy donor leukapheresis cones obtained pre UK COVID-19 pandemic (March 2019 to Jan 2020, NHS Blood and Transplant, UK) by density gradient separation.

Single Chain Trimers

Single chain trimer constructs were made and tested as previously described (*7, 11*). Expression relative to the control construct (which encoded the peptide VMAPRTLLL) was calculated from median fluorescent intensity (MFI) of the transfected cells, corrected by subtracting the MFI of mock transfected cells.

HLA-E binding peptide-exchange ELISA assay

A sensitive HLA-E binding ELISA assay was performed as described with minor optimization (*11, 12*). Briefly, refolded HLA-E proteins (0.5μM) preloaded with a labile VL9 variant peptide (7MT2) was incubated in the presence of excess SARS-CoV-2 derived peptides at 100μM. The exchange reaction took place overnight in buffer comprising 400mM L-arginine monohydrochloride, 100mM Tris, 5mM reduced glutathione, 0.5mM oxidized Glutathione and 2 mM EDTA. The reaction was diluted 1:100 in phosphate buffered saline (PBS)-2% bovine serum albumin (BSA) and 50 μL was added to ELISA plates pre-coated with 20μg/mL anti-

human HLA-E mAb (3D12, Biolegend). After 1 hour, plates were washed with PBS/0.05%Tween-20 and incubated with 2μg/mL anti-human β2M horseradish peroxidase (HRP)-conjugated IgG antibodies for 30 mins. Following subsequent wash steps, 50μL enhancement reagent (Dako EnVision, diluted in PBS/2%BSA with 1% normal mouse serum) was added to amplify the HRP signal. 100μL TMB substrate was added for development and the reaction was terminated with 100μL STOP Solution. Absorbance at 450nm was read using a FLUOstar OMEGA reader. Three independent peptide-exchange reactions per peptide were included per test, with 2 duplicates from each reaction tested in the ELISA assay. Each run comprised VL9 positive control and a peptide-free no-rescue control to normalize the background and to express the binding affinity as %VL9. The HLA-E binding rankings were calculated as (average tested peptide signals-average DMSO signals)/ (average VL9 signals-average DMSO signals).

HLA-E tetramers generation and staining of $CD8^+$ T cells

UV peptide exchange HLA-E*01:03-biotinylated monomers were conjugated to streptavidin-bound PE, APC or BV421 at a Molar ratio of 4:1 as described (*5*). Conventional tetramers were additionally prepared for P001 (VMPLSAPTL). PBMCs from COVID-19 patients were stained with conventional or UV-exchanged tetramers at 0.5ug per $1x10^6$ cells for 45 minutes at room temperature (RT) in the dark. Upon washing with PBS, cells were subsequently stained with Live/Dead Fixable Aqua and flow antibodies to surface markers for 20 min at RT in the dark. Alternatively, the modified wash procedure was taken as the wash step before surface antibody staining was omitted as indicated. Cells were then washed and fixed with 2% paraformaldehyde, and then acquired using a LSR Fortessa (BD Biosciences). The data were analyzed using FlowJo software v10.4 (Tree Star).

Live cell sorting and cloning of HLA-E tetramer positive CD8$^+$T cells

PBMCs from convalescent patients were stained with HLA-E tetramers initially. Cells were subsequently washed with PBS and stained with Live/Dead Fixable Aqua, anti-CD3–APC-Cy7, anti-CD4–PerCP-Cy5.5, anti-CD8-BV421, anti-CD94-FITC and anti-CD56-BV510 for 30 mins at RT in the dark. CD3$^+$CD4$^-$CD56$^-$CD94$^-$CD8$^+$Tetramer$^+$ T cells were live sorted using FACSAria III (BD Biosciences). Sorted cells were seeded into 384-well plates at 0.4 cells per well with irradiated (45 Gy) allogeneic feeder cells (3 healthy donors, 2x10^6 cells/mL) stimulated with PHA (1μg/mL) and IL-2 (500 U/mL) cultured in complete media (CM) containing RPMI 1640, 10% AB human sera (UK National Blood Service), 1% penicillin/streptomycin, 1% glutamine, 1% sodium pyruvate, 1% non-essential amino acids, 0.1% beta-mercaptoethanol. 12 days later, T cell clones were further expanded with feeder cells and PHA/IL-2. Tetramer positivity was tested using HLA-E tetramers (APC-, BV421- or PE-conjugated) and anti-CD3-APC-Cy7, anti-CD8-BV421, and Live/Dead Fixable Aqua. Functions of CD8 clones were subsequently assessed using intracellular staining described below.

Functional assessment of SARS-CoV-2 specific CD8$^+$T cells

To evaluate the functions of CD8 clones, cells were rested in CM before coculture with a genetically modified K562 cell line (HLA-E-expressing, classical HLA-I null) incubated overnight with peptides (50μM) at 27℃. The coculture was incubated at the CD8: K562 ratio of 1:3 for 9 hours. For maximal functionality testing, CD8 clones were also independently treated with PMA/Ionomycin. Brefeldin A (5μg/ml) and GolgiStop (5μg/ml) were added after 1 hour during incubation. Anti-CD107a-BV421 and anti-CD107b-BV421 were supplemented at beginning of coculture. Cells were stained with Live/Dead Fixable Aqua and flow antibodies surface markers (anti-human CD3 and anti-human CD8) in PBS, and then fixed and

permeabilized with Cytofix/Cytoperm (BD Biosciences). Intracellular staining (ICS) was performed with flurochrome-conjugated antibodies against TNFα, IFN-γ, MIP-1β, IL-4, IL-13, CTLA-4 and CD137 in Permwash solution. Cells were acquired on a LSRFortessa (BD Biosciences) and analyzed using FlowJo v10.4 (Tree Star).

TCR sequencing

Total RNA of CD8 clones was extracted using a RNeasy Plus Mini Kit (Qiagen). TCR libraries using around 100ng RNA were prepared using a SMARTer Human TCR a/b Profiling Kit (Takara Bio) according to the manufacturer instructions based on SMART (*28*) and 5'RACE techniques (*29*). Subsequently, full length TCR alpha and beta chains were sequenced using a Miseq Reagent Kit v3 (600-cycle) on an Miseq sequencer (Illumina). Raw BCL files were converted to FASTQ format using bcl2fastq (v2.20.0.422). TCR sequences were then reconstructed using MiXCR (v3.0.13) (*48*), using the mixcr analyze amplicon command, and only productive TCRs were included. MiXCR output files were parsed into R (v4.0.1) using tcR (v2.3.2). TCRs were filtered based on clone counts to retain only 1α1β or 2α1β paired TCRs for each clone. Clonality was confirmed by the uniqueness of TCR sequences, where each clone showed only one TCR β chain (Table 1).

Viral suppression assay

The SARS-CoV-2 viral strain, Victoria 01/20 (BVIC01), was used to infect Calu-3 cells (*40, 49*) (provided by PHE Porton Down after the provision from the Doherty Centre Melbourne, Australia). Briefly, $1x10^5$ Calu-3 cells were seeded in flat-bottom 96-well plates 48 hours prior to infection with SARS-CoV-2 at the indicated MOIs for 2h. The viral inoculum was carefully removed and subsequently washed with advanced DMEM supplemented with 10% FBS, 1% GlutaMAX, 1% Sodium Pyruvate and 1%PS. CD8+ T cells were then added at E:T of 1:1 or

4:1. Upon 15 hours post-infection (hpi), Calu-3 cells were washed with PBS thoroughly to remove CD8+ T cells. The VSA was carried out in duplicates for each condition. RNA lysates of infected Calu3 cells from each condition were then pooled for RNA extraction using a RNeasy Plus Mini Kit (Qiagen). Total RNA was then subject to one-step RT-qPCR to measure cellular viral transcription using the StepOne Real-Time PCR System (Applied Biosystem). Takyon One-Step RT Probe Mastermix (Eurogentec) and primers/probes from SARS-CoV-2 CDC EUA Kit (IDT) were used under the following PCR conditions: 50°C for 30 min, 95°C for 2 min, then anneal and extension of 95°C for 5 sec and 60°C for 30 secs running in total of 45 cycles. β2M gene (Thermofisher) was detected as the endogenous control. SARS-CoV-2 infected Calu-3 cells without CD8+ T cell coculture were used as controls.

Detection of HLA-E and HLA-I expression after SARS-CoV-2 infection

Calu-3 or A549 cells overexpressing human ACE2 were tested for HLA expression after SARS-CoV-2 infection. In brief, cells were first seeded 48 hours before SARS-CoV-2 infection at the indicated MOIs (0.01, 0.1 and 1) for 2 hours. Unbound virus was removed by washing and cells were incubated with fresh culture media supplemented with or without Remdesivir (10μM). At indicated time points (6h, 12h, 24h and 48h), cells were washed with PBS, trypsinized and maintained on ice for 30 min. The viability of Calu-3 cells was confirmed to be >99% using LIVE/DEAD Fixable Aqua Dead Cell Stain Kit. Surface or ICS staining was performed to detect surface or total HLA-E or HLA-I expression using anti-human HLA-E antibody (3D12, Biolegend) and anti-human HLA-I antibody (W6/32, Biolegend). Infected cells were detected by anti-SARS-CoV-2-spike antibody (R&D). Cells were acquired on a LSRFortessa (BD Biosciences) and analyzed using FlowJo v10.4 (Tree Star).

Cloning of single chain NKG2x-CD94 soluble ectodomains

A NKG2x-CD94 ectodomain interspersed with a flexible (GGS)2 linker was cloned by splicing overlap extension PCR (Q5 Hot Start polymerase, NEB). Primers AgeI-5' NKG2x: CATGACCGGTACACAGAAAGCGCGTCATTG and 3' NKG2x GGS2: GCTACCGCCGCTACCGCCAAGCTTATGCTTACAATGATA were used to generate the NKG2x-GGS portion, and 5' GGS2 CD94: GGCGGTAGCGGCGGTAGCATTGAGCCTGCCTTTACAC plus 3' CD94-KpnI: AGTCGGTACCTATCAGCTGCTGTTTGCAGATGTATCTG produced the GGS-CD94 portion. A second PCR step was performed on the combined initial PCR products using the external AgeI-5' NKG2x - 3' CD94-KpnI primers. Following subcloning into a pCR-Blunt-II-TOPO shuttle vector (Invitrogen), the product was digested (AgeI and KpnI) and cloned into the pHLSec-Avitag3 expression vector [50]. DH5α *E.coli* were used for plasmid propagation and sequence analysis (QIAgen miniprep and maxiprep kits).

Expression and Purification of NKG2x-CD94 fusion proteins

Biotinylated NKG2x-CD94 fusion protein was expressed using the Expi293 system (ThermoFisher Scientific). Biotinylation was achieved by co-transfection with a BirA enzyme-encoding pHL-BirA-KDEL vector (10:1 NKG2x:BirA vector ratios), in media supplemented with 2 mM D-biotin. At 96 hours post-transfection, supernatants were clarified (by centrifugation and 0.45µM PES membrane filtration), adjusted to IMAC binding conditions (20mM NaPi pH8.0, 0.5M NaCl, 20mM Imidazole) and loaded onto a HisTrap FF 5ml Ni-NTA column on an AKTA Pure FPLC system (Cytiva). Protein was eluted with 5CV Elution buffer (20mM NaPi pH8.0, 0.5M NaCl, 300mM Imidazole), and fractions were pooled, concentrated and subsequently loaded onto a Superdex 200 Increase 10/300 GL chromatography column equilibrated with 20mM Tris-HCl pH8.0 150mM NaCl. Size-

fractionated samples were analysed by SDS-PAGE, and biotinylation was assessed using a streptavidin shift assay.

NKG2x-CD94 Tetramer staining and flow cytometry

Streptavidin-APC tetramerised NKG2x-CD94 material was used to stain Δβ2m 293T cells expressing single chain trimer constructs encoding peptide, β2m and HLA-E heavy chain fused to EGFP. Cells were grown to approximately 60-70% confluency prior to transient transfection using Genejuice reagent (Merck Millipore). Following EGFP expression validation at 24h post-transfection, cells were harvested, washed in ice-cold PBS and co-stained with 100ng of tetramerised NKG2x-CD94 plus 1µl of anti-β_2m mAb 2M2-PEcy7 (BioLegend), in a final volume of 100µl of PBS, for 20 minutes at 4°C. Cells were then washed and resuspended in PBS for flow cytometry using a CyAn ADP flow cytometer (Beckman Coulter). Analysis was conducted using FlowJo 10 software (Becton Dickinson).

Statistical analysis

Data analysis was performed, and graphs were generated using GraphPad Prism v8. Mann Whitney test was adopted to compare difference between 2 groups where applicable.

References and Notes:

1. R. K. Strong *et al.*, HLA-E allelic variants. Correlating differential expression, peptide affinities, crystal structures, and thermal stabilities. *J Biol Chem* **278**, 5082-5090 (2003).
2. R. Apps *et al.*, Relative expression levels of the HLA class-I proteins in normal and HIV-infected cells. *J Immunol* **194**, 3594-3600 (2015).
3. V. M. Braud, D. S. Allan, D. Wilson, A. J. McMichael, TAP- and tapasin-dependent HLA-E surface expression correlates with the binding of an MHC class I leader peptide. *Curr Biol* **8**, 1-10 (1998).
4. G. Camilli *et al.*, Regulation and trafficking of the HLA-E molecules during monocyte-macrophage differentiation. *J Leukoc Biol* **99**, 121-130 (2016).
5. V. M. Braud *et al.*, HLA-E binds to natural killer cell receptors CD94/NKG2A, B and C. *Nature* **391**, 795-799 (1998).
6. J. D. Miller *et al.*, Analysis of HLA-E peptide-binding specificity and contact residues in bound peptide required for recognition by CD94/NKG2. *J Immunol* **171**, 1369-1375 (2003).
7. S. G. Hansen *et al.*, Broadly targeted CD8(+) T cell responses restricted by major histocompatibility complex E. *Science* **351**, 714-720 (2016).
8. A. S. Heinzel *et al.*, HLA-E-dependent presentation of Mtb-derived antigen to human CD8+ T cells. *J Exp Med* **196**, 1473-1481 (2002).
9. S. A. Joosten *et al.*, Mycobacterium tuberculosis peptides presented by HLA-E molecules are targets for human CD8 T-cells with cytotoxic as well as regulatory activity. *PLoS Pathog* **6**, e1000782 (2010).
10. C. Romagnani *et al.*, HLA-E-restricted recognition of human cytomegalovirus by a subset of cytolytic T lymphocytes. *Hum Immunol* **65**, 437-445 (2004).
11. L. C. Walters *et al.*, Pathogen-derived HLA-E bound epitopes reveal broad primary anchor pocket tolerability and conformationally malleable peptide binding. *Nat Commun* **9**, 3137 (2018).
12. L. C. Walters, A. J. McMichael, G. M. Gillespie, Detailed and atypical HLA-E peptide binding motifs revealed by a novel peptide exchange binding assay. *Eur J Immunol*, (2020).
13. D. Malouli *et al.*, Cytomegaloviral determinants of CD8(+) T cell programming and RhCMV/SIV vaccine efficacy. *Sci Immunol* **6**, (2021).
14. M. C. Verweij *et al.*, Modulation of MHC-E transport by viral decoy ligands is required for RhCMV/SIV vaccine efficacy. *Science* **372**, (2021).
15. J. E. Grotzke *et al.*, The Mycobacterium tuberculosis phagosome is a HLA-I processing competent organelle. *PLoS Pathog* **5**, e1000374 (2009).
16. V. Jurtz *et al.*, NetMHCpan-4.0: Improved Peptide-MHC Class I Interaction Predictions Integrating Eluted Ligand and Peptide Binding Affinity Data. *J Immunol* **199**, 3360-3368 (2017).
17. M. Toebes, B. Rodenko, H. Ovaa, T. N. Schumacher, Generation of peptide MHC class I monomers and multimers through ligand exchange. *Curr Protoc Immunol* **Chapter 18**, Unit 18 16 (2009).
18. M. H. Lampen *et al.*, Alternative peptide repertoire of HLA-E reveals a binding motif that is strikingly similar to HLA-A2. *Mol Immunol* **53**, 126-131 (2013).

19. N. Le Bert *et al.*, SARS-CoV-2-specific T cell immunity in cases of COVID-19 and SARS, and uninfected controls. *Nature* **584**, 457-462 (2020).
20. A. Grifoni *et al.*, Targets of T Cell Responses to SARS-CoV-2 Coronavirus in Humans with COVID-19 Disease and Unexposed Individuals. *Cell* **181**, 1489-1501 e1415 (2020).
21. B. J. Meckiff *et al.*, Imbalance of Regulatory and Cytotoxic SARS-CoV-2-Reactive CD4(+) T Cells in COVID-19. *Cell* **183**, 1340-1353 e1316 (2020).
22. Y. Peng *et al.*, Broad and strong memory CD4(+) and CD8(+) T cells induced by SARS-CoV-2 in UK convalescent individuals following COVID-19. *Nat Immunol* **21**, 1336-1345 (2020).
23. C. Rydyznski Moderbacher *et al.*, Antigen-Specific Adaptive Immunity to SARS-CoV-2 in Acute COVID-19 and Associations with Age and Disease Severity. *Cell* **183**, 996-1012 e1019 (2020).
24. D. Schub *et al.*, High levels of SARS-CoV-2-specific T cells with restricted functionality in severe courses of COVID-19. *JCI Insight* **5**, (2020).
25. A. P. Ferretti *et al.*, Unbiased Screens Show CD8(+) T Cells of COVID-19 Patients Recognize Shared Epitopes in SARS-CoV-2 that Largely Reside outside the Spike Protein. *Immunity* **53**, 1095-1107 e1093 (2020).
26. J. Fajnzylber *et al.*, SARS-CoV-2 viral load is associated with increased disease severity and mortality. *Nat Commun* **11**, 5493 (2020).
27. S. Zheng *et al.*, Viral load dynamics and disease severity in patients infected with SARS-CoV-2 in Zhejiang province, China, January-March 2020: retrospective cohort study. *BMJ* **369**, m1443 (2020).
28. S. Picelli *et al.*, Full-length RNA-seq from single cells using Smart-seq2. *Nat Protoc* **9**, 171-181 (2014).
29. Y. Zhao *et al.*, Primary human lymphocytes transduced with NY-ESO-1 antigen-specific TCR genes recognize and kill diverse human tumor cell lines. *J Immunol* **174**, 4415-4423 (2005).
30. H. Yang *et al.*, HLA-E-restricted, Gag-specific CD8(+) T cells can suppress HIV-1 infection, offering vaccine opportunities. *Sci Immunol* **6**, (2021).
31. J. Huang *et al.*, Detection, phenotyping, and quantification of antigen-specific T cells using a peptide-MHC dodecamer. *Proc Natl Acad Sci U S A* **113**, E1890-1897 (2016).
32. G. Dolton *et al.*, Optimized Peptide-MHC Multimer Protocols for Detection and Isolation of Autoimmune T-Cells. *Front Immunol* **9**, 1378 (2018).
33. M. M. Davis *et al.*, Ligand recognition by alpha beta T cell receptors. *Annu Rev Immunol* **16**, 523-544 (1998).
34. M. Corr *et al.*, T cell receptor-MHC class I peptide interactions: affinity, kinetics, and specificity. *Science* **265**, 946-949 (1994).
35. K. Matsui, J. J. Boniface, P. Steffner, P. A. Reay, M. M. Davis, Kinetics of T-cell receptor binding to peptide/I-Ek complexes: correlation of the dissociation rate with T-cell responsiveness. *Proc Natl Acad Sci U S A* **91**, 12862-12866 (1994).
36. T. Einav, S. Yazdi, A. Coey, P. J. Bjorkman, R. Phillips, Harnessing Avidity: Quantifying the Entropic and Energetic Effects of Linker Length and Rigidity for Multivalent Binding of Antibodies to HIV-1. *Cell Syst* **9**, 466-474 e467 (2019).
37. G. Denkberg, C. J. Cohen, Y. Reiter, Critical role for CD8 in binding of MHC tetramers to TCR: CD8 antibodies block specific binding of human tumor-specific MHC-peptide tetramers to TCR. *J Immunol* **167**, 270-276 (2001).

38. L. G. Thorne *et al.*, SARS-CoV-2 sensing by RIG-I and MDA5 links epithelial infection to macrophage inflammation. *EMBO J*, e107826 (2021).
39. M. Hoffmann *et al.*, SARS-CoV-2 Cell Entry Depends on ACE2 and TMPRSS2 and Is Blocked by a Clinically Proven Protease Inhibitor. *Cell* **181**, 271-280 e278 (2020).
40. P. A. C. Wing *et al.*, Hypoxic and pharmacological activation of HIF inhibits SARS-CoV-2 infection of lung epithelial cells. *Cell Rep* **35**, 109020 (2021).
41. Y. Zhang *et al.*, The ORF8 protein of SARS-CoV-2 mediates immune evasion through down-regulating MHC-Iota. *Proc Natl Acad Sci U S A* **118**, (2021).
42. Y. Li *et al.*, SARS-CoV-2 induces double-stranded RNA-mediated innate immune responses in respiratory epithelial-derived cells and cardiomyocytes. *Proc Natl Acad Sci U S A* **118**, (2021).
43. J. C. Hsu, M. Laurent-Rolle, J. B. Pawlak, C. B. Wilen, P. Cresswell, Translational shutdown and evasion of the innate immune response by SARS-CoV-2 NSP14 protein. *Proc Natl Acad Sci U S A* **118**, (2021).
44. Z. Silva *et al.*, MHC Class I Stability is Modulated by Cell Surface Sialylation in Human Dendritic Cells. *Pharmaceutics* **12**, (2020).
45. L. C. Walters *et al.*, Distinct structural configurations and conformational ensembles distinguish canonical leader peptide-versus pathogen epitope-bound HLA-E. *Journal and Preprint Server submitted*, (2021).
46. O. P. Joffre, E. Segura, A. Savina, S. Amigorena, Cross-presentation by dendritic cells. *Nat Rev Immunol* **12**, 557-569 (2012).
47. R. Anjanappa *et al.*, Structures of peptide-free and partially loaded MHC class I molecules reveal mechanisms of peptide selection. *Nat Commun* **11**, 1314 (2020).
48. D. A. Bolotin *et al.*, MiXCR: software for comprehensive adaptive immunity profiling. *Nat Methods* **12**, 380-381 (2015).
49. L. Caly *et al.*, Isolation and rapid sharing of the 2019 novel coronavirus (SARS-CoV-2) from the first patient diagnosed with COVID-19 in Australia. *Med J Aust* **212**, 459-462 (2020).

Acknowledgements: We thank the patients and their loved ones who volunteered to contribute to this study at one of the most difficult times in their lives, and the research staff at each hospital who recruited patients at personal risk during the most extreme conditions ever witnessed in UK hospitals. This work also uses data provided by patients and collected by the NHS as part of their care and support #DataSavesLives. We are grateful to Claudia Rubio for excellent technical assistance and William James (Sir William Dunn School of Pathology, University of Oxford) for generous provision of SARS-CoV-2 strains. Calu-3 cells were kindly provided by Anderson Ryan (Oncology Department, University of Oxford). A549-ACE2 cells were kindly provided by Alfredo Castello (CVR, University of Glasgow). The pHLSec-Avitag3 vector was a kind gift from Prof. Radu Aricescu (MRC LMB, Cambridge).

Funding:

the Bill and Melinda Gates Foundation (BMGF OPP1133649)

the Chinese Academy of Medical Sciences (CAMS) Innovation Fund for Medical Sciences (CIFMS 2018-I2M-2-002)

the UK Medical Research Council (MRC) funded Human Immunology Unit, MRC project grant MR/R022011/1

the Oxfordshire Health Services Research Committee reference 1308, NIHR Biomedical Research Centre, Oxford, Department of Health and Social Care UKRI/NIHR COVID-19 Rapid Response Grant (COV!9-RECPLA)

Wellcome Trust grant 109965MA

CIFMS 2018-I2M-2-002 and the China Scholarship Council (HS)

Wellcome Trust Investigator Award (IA) 200838/Z/16/Z (JMcK)

Wellcome Trust fellowship [205228/Z/16/Z] (LT)

the National Institute for Health Research Health Protection Research Unit (HPRU) in Emerging and Zoonotic Infections (NIHR200907) at University of Liverpool in partnership with Public Health England (PHE), in collaboration with Liverpool School of Tropical Medicine and the University of Oxford (LT)

AJM is an NIHR Academic Clinical Lecturer, and AJM and PB are Jenner Institute Investigators

NIHR Senior Investigator Award (award 201385) (P.J.M.O.)

ISARIC4C is supported by grants from the Medical Research Council (grant MC_PC_19059), the National Institute for Health Research (NIHR) (award CO-CIN-01) and by the NIHR Health Protection Research Unit (HPRU) in Emerging and Zoonotic Infections at University of Liverpool in partnership with Public Health England (PHE), in collaboration with Liverpool School of Tropical Medicine and the University of Oxford (award 200907), NIHR HPRU in Respiratory Infections at Imperial College London with PHE (award 200927), Wellcome Trust and Department for International Development (215091/Z/18/Z), and the Bill and Melinda Gates Foundation (OPP1209135), the Liverpool Experimental Cancer Medicine Centre (grant reference: C18616/A25153), NIHR Biomedical Research Centre at Imperial College London (IS-BRC-1215-20013), and the NIHR Clinical Research Network provided infrastructure support for this research.

Author contributions:

Study design, experiment performance, data analysis and manuscript writing: HS, HBY, GMG, JMcK, AJMcM

Critical manuscript and data review: PB, PK

HLA-E binding peptides prediction and testing: SB, LW, GMG

SCT, DSF assays and protein production: SB, LG, MQ

CL3 laboratory experiments: XDZ, PACW

TCR sequencing and analysis: XY, SLF, YCP, TD

Patient sample provision: TD, SM, MGS, LCQT, PJMO, JKB, AJM, PK and ISARIC4C

All authors read and approved the manuscript.

Competing interests: The authors declare no competing interests.

Data and materials availability: All data are available in the main text or the supplementary materials.

Table 1. TCR usage of HLA-E restricted SARS-CoV-2 specific CD8 T cell clones

Clone	Epitope	CDR3_alpha	TRAV	TRAJ	TCRα reads *	CDR3_beta	TRBV	TRBJ	TCRβ reads *
1106 C01	P001	CAVSDTGNQFYF	TRAV21	TRAJ49	99%	CASSLFGGAHGYTF	TRBV11-2	TRBJ1-2	98%
1106 C05	P001	CALGEGYTGANSKLTF	TRDV1	TRAJ56	100%	CAWSVVGQGAPRYGYTF	TRBV30	TRBJ1-2	99%
1504 C43	P001	CAVGASDGQKLLF	TRAV21	TRAJ16	95%	CASRPRGSGTGELFF	TRBV7-9	TRBJ2-2	94%
1106 C04	P006	CVVNPLTNFGNEKLTF	TRAV12-1	TRAJ48	94%	CASSTEVSTNEKLFF	TRBV27	TRBJ1-4	98%
1106 C37	P006	CAVRSSGGSYIPTF	TRAV1-2	TRAJ6	99%	CASSTGDSNQPQHF	TRBV3-1	TRBJ1-5	99%
1106 C03	P015	CVVNPNNDMRF CAMRGSDKLIF	TRAV12-1 TRAV14DV4	TRAJ43 TRAJ34	50% 50%	CASSEDSFLNTEAFF	TRBV6-1	TRBJ1-1	100%
1106 C16	P015	CAVGNQAGTALIF	TRAV8-3	TRAJ15	99%	CASSYNPSSGEAFF	TRBV6-5	TRBJ1-1	100%
1106 C32	P015	CAESTDTGRRALTF	TRAV5	TRAJ5	100%	CSVEGQGAPGYTF	TRBV29-1	TRBJ1-2	100%
1106 C08	P015	CALYTGGFKTIF	TRAV17	TRAJ9	100%	CASRSGGLDEQFF	TRBV19	TRBJ2-1	99%
1504 C03	P015	CAVPSGTYKYIF	TRAV5	TRAJ40	100%	CASRTRQPGLGNNEQFF	TRBV6-5	TRBJ2-1	100%
1504 C24	P015	CAVEEGFQKLVF CILRDWDGTASKLTF	TRAV22 TRAV26-2	TRAJ8 TRAJ44	51% 48%	CASSQDSGNEQFF	TRBV4-1	TRBJ2-1	98%
1504 C09	P015	CAESAYGGSQGNLIF	TRAV5	TRAJ42	99%	CASSAGETQYF	TRBV25-1	TRBJ2-5	99%
1106 C17	P015	CAMREERNARLMF CAVRDGGGYGGATNKLIF	TRAV14DV4 TRAV3	TRAJ31 TRAJ32	85% 14%	CASSHSTGVYEQYF	TRBV7-9	TRBJ2-7	100%

*Total reads from TCR sequencing were 81576 (median, IQR: 40624-161076).

Aug 11 2021

Supplementary Materials:

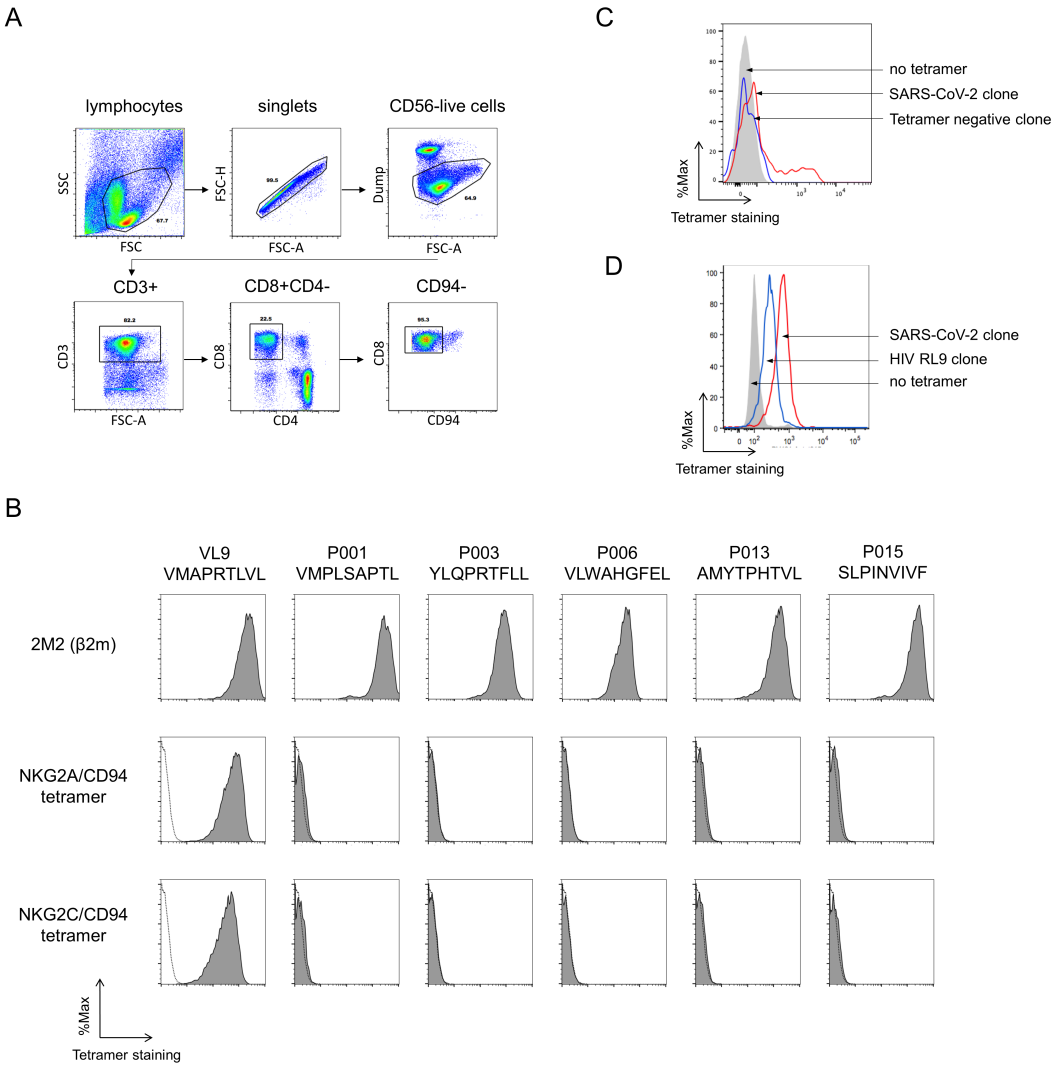

Fig. S1. Identification of HLA-E restricted SARS-CoV-2-specific CD8 cells

(A) Representative graphs show the gating strategy to analyze tetramer positive cells. Live CD3+CD4-CD8+ cells were gated and CD56-CD94- cells were selected for evaluation. **(B)** Lack of NKG2A-CD94 or NKG2C-CD94 tetramer binding to HLA-E bound SARS CoV-2 peptides. Representative flow cytometry histograms (two independent experiments) are shown for anti-β2m antibody staining (top row), NKG2A-CD94 tetramer staining (middle row) and NKG2C-CD94 tetramer staining (bottom row) of SARS-2 peptide – HLA-E transfected β 2m-knockout 293T cells. Respective peptides are shown at the top of each column, with the VL9 HLA-leader peptide as a control. Filled histograms show staining with each respective reagent. Dotted lines show staining of EGFP controls for the two tetramers. **(C-D)**, Representative SARS-CoV-2 CD8 clones underwent the normal tetramer staining procedure (**C**) or a modified-wash procedure (**D**), as outlined in the Methods section. The histograms depict the intensity of tetramer staining of a SARS-CoV-2 CD8 clone (red), an irrelevant HLA-E-restricted HIV-specific CD8 clone, a tetramer negative clone (blue) and a no tetramer staining control (grey).

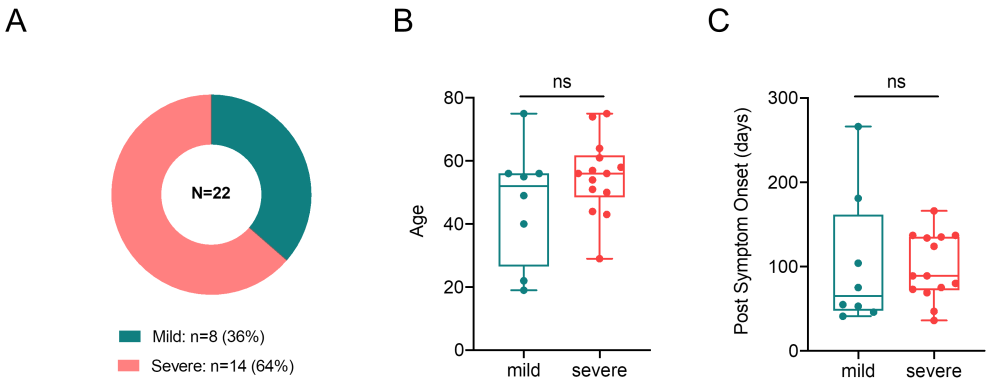

Fig. S2. Description of the cohort of convalescent COVID-19 patients

(A) The pie chart depicts the composition of mild versus severe patients. Mild, green; Severe, red. The mild and severe patients did not differ in terms of age (**B**) or post symptom onset (**C**).

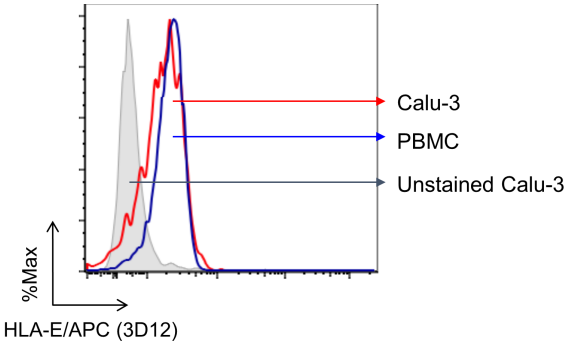

Fig. S3. HLA-E expression of Calu-3 cells

The flow histogram illustrates surface HLA-E expression on Calu-3 cells compared to PBMCs from a healthy donor, measured by 3D12 staining (x-axis). Calu-3 cells, red curve; PBMCs, blue curve; unstained Calu-3 cells, grey shade.

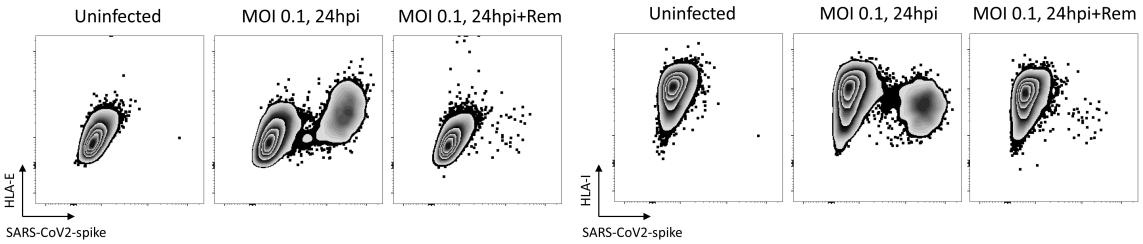

Fig. S4. HLA-E and HLA-I expression of Calu-3 cells after SARS-CoV-2 infection and Remdesivir treatment

Representative flow graphs showing FACS plot of HLA-E (anti-3D12) or HLA-I (anti-W6/32) staining (y-axis) versus SARS-CoV-2 spike expression (x-axis) of Calu-3 cells after SARS-CoV-2 infection (MOI 0.1) and following Remdesivir treatment. hpi = hours post infection.

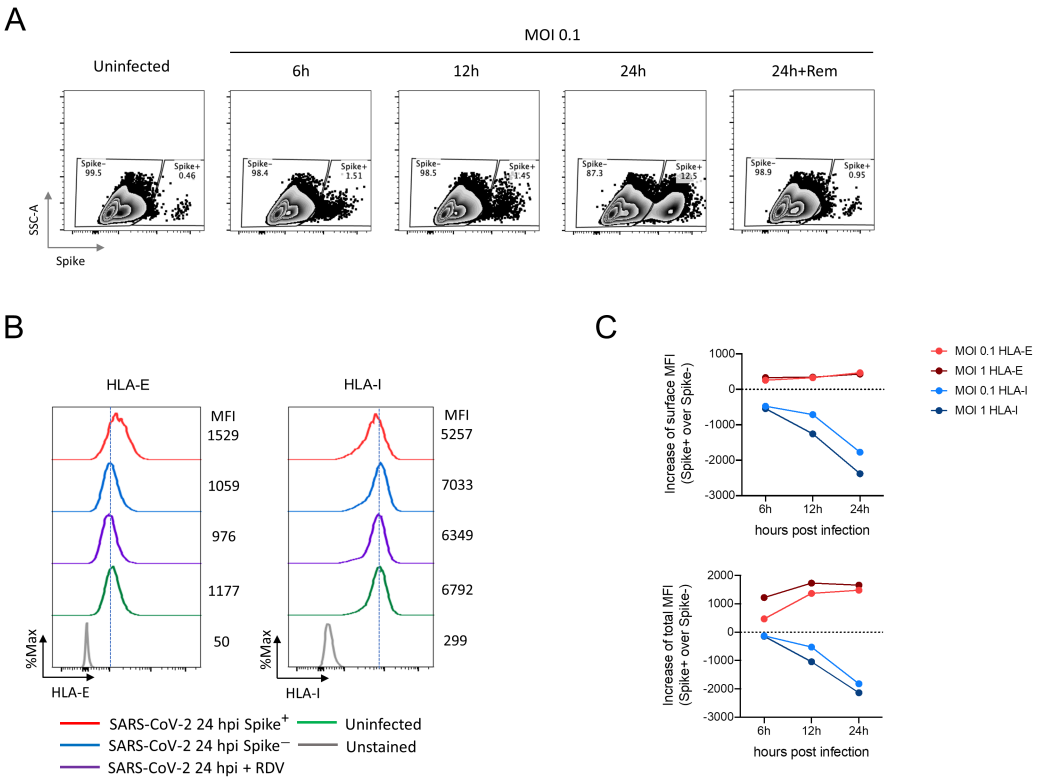

Fig. S5. HLA-E and HLA-I dysregulation on SARS-CoV-2 infected hACE-2-expressing A549 cells

(A-B), Replication dynamics of SARS-CoV-2 in A549-ACE2 cells is assessed using an anti-SARS-CoV-2 spike antibody following infection with SARS-CoV-2 (Victoria 01/20 strain) at MOI 1 and 0.1 at 6, 12, 24 hpi. **(A)** Representative graphs depict spike^{+}cells in MOI 0.1 against SSC by ICS. The infection is blocked by supplementing Remdesivir (Rem) after viral infection. **(B)** HLA-E and HLA-I surface expression in each condition at 24hpi under MOI 0.1 is shown. Spike+, red; Spike-, blue; Remdesivir, purple; Uninfected control, green; Unstained, grey. The value of MFI is indicated in the right. **(C)** HLA-E and HLA-I expression in spike+ versus spike- cells change dynamically along with time. MOI 0.1, red (HLA-E) and blue (HLA-I); MOI 1, cayenne (HLA-E) and ocean (HLA-I).

Table S1. Description of 9-mer predicted peptides of SARS-CoV-2

Peptide ID	Amino acid sequence	Start position	Location
P001	VMPLSAPTL	5556	ORF1ab
P002	VMYASAVVL	3683	ORF1ab
P003	YLQPRTFLL	269	Spike
P004	MMISAGFSL	6425	ORF1ab
P005	YQPYRVVVL	505	Spike
P006	VLWAHGFEL	6109	ORF1ab
P007	YMPYFFTLL	2168	ORF1a
P008	LMPLKAPKE	730	ORF1a
P009	YMPASWVMR	3654	ORF1a
P010	HKPPISFPL	5399	ORF1ab
P011	WVPRASANI	423	ORF1ab
P012	LLADKFPVL	6246	ORF1ab
P013	AMYTPHTVL	5315	ORF1ab
P014	AQLPAPRTL	5727	ORF1ab
P015	SLPINVIVF	2535	ORF1ab
P016	QMAPISAMV	2373	ORF1ab
P017	AAGLEAPFL	98	ORF3a
P018	SAPHGVVFL	1055	SPIKE
P019	HVQLSLPVL	13	ORF1ab
P020	VVPGLPGTI	2865	ORF1ab
P021	FLPFAMGII	3611	ORF1ab
P022	FLLPSLATV	3639	ORF1ab
P023	ILGLPTQTV	5849	ORF1ab
P024	IAPGQTGKI	410	SPIKE
P025	DAVRDPQTL	574	SPIKE
P026	HFPREGVFV	1088	SPIKE
P027	QLPAPRTLL	5728	ORF1ab
P028	VQPQLEMEL	1008	ORF1ab
P029	LQLPQGTTL	159	NP

Table S2. Characteristics of the convalescent COVID-19 patients

Patient ID	age	sex	Post symptom onset	Disease type
Pt023	47	Male	42	mild
Pt1007	95	Female	43	mild
Pt1016	25	Female	46	mild
Pt1105	57	Male	41	severe
Pt1504	60	Male	42	severe
CCP01118	55	Female	53	Mild
CCP01122	56	Female	41	Mild
CCP01168*	58	Female	124	Severe
CCP01205	56	Female	46	Mild
CCP01206	56	Male	36	Severe
CCP01526	61	Male	47	Severe
CCP01529	49	Female	55	Mild
CCP01725*	54	Female	137	Severe
CCP01731*	51	Male	135	Severe
CCP01734	64	Male	166	Severe
CCP01737*	75	Male	137	Severe
CCP01752	57	Male	69	Severe
CCP01758	56	Male	75	Severe
CCP01942	43	Male	89	Severe
CCP01945	44	Male	89	Severe
CCP02173*	50	Female	134	Severe
CCP02272	75	Male	181	Mild

CCP02276	74	Male	73	Severe
CCP02294	40	Female	266	Mild
CCP02336	29	Female	80	Severe
CCP02344	22	Male	104	Mild
CCP02366*	19	Female	75	Mild

*The patients are HLA-A2 positive.

Table S3. Summary of the 13 SARS-CoV-2 Tetramer Binding T cell clones

Clone ID	Tetramer staining (%)	Specificity	Highest peptide response	Virus Suppression in Calu3 cells (%)		T Cell Receptor			
				E:T 1:1	E:T 4:1	TRAV	TRAJ	TRBV	TRBJ
1106C1	35.0	P001	nt	75.87	96.16	TRAV21	TRAJ49	TRBV11-2	TRBJ1-2
1106C3	0.97	P015	CD137	96.15	96.61	TRAV12-1 TRAV14DV4	TRAJ43 TRAJ34	TRBV6-1	TRBJ1-1
1106C4	37.8	P006	nt	82.51	96.97	TRAV12-1	TRAJ48	TRBV27	TRBJ1-4
1106C5	3.2	P001	Granzyme	82.43	93.02	TRDV1	TRAJ56	TRBV30	TRBJ1-2
1106C8	8.07	P015	nt	71.77	93.89	TRAV17	TRAJ9	TRBV19	TRBJ2-1
1106C16	41.9	P015	nt	85.24	93.48	TRAV8-3	TRAJ15	TRBV6-5	TRBJ1-1
1106C17	16.0	P015	nt	76.74	93.32	TRAV14DV4 TRAV3	TRAJ31 TRAJ32	TRBV7-9	TRBJ2-7
1106C32	2.19	P015	CD107	81.7	91.48	TRAV5	TRAJ5	TRBV29-1	TRBJ1-2
1106C37	0.78	P006	CD107	nt	nt	TRAV1-2	TRAJ6	TRBV3-1	TRBJ1-5
1504C3	1.06	P015	CD107	75.95	91.26	TRAV5	TRAJ40	TRBV6-5	TRBJ2-1
1504C9	1.04	P015	nt	52.96	54.84	TRAV5	TRAJ42	TRBV25-1	TRBJ2-5
1504C24	1.09	P015	nt	56.11	81.95	TRAV22 TRAV26-2	TRAJ8 TRAJ44	TRBV4-1	TRBJ2-1
1504C43	0.93	P001	CD107	nt	nt	TRAV21	TRAJ16	TRBV7-9	TRBJ2-2